TRANSIENT SPATIOTEMPORAL CHAOS IN A DIFFUSIVELY AND SYNAPTICALLY COUPLED MORRIS-LECAR NEURONAL NETWORK

By

Jacopo Lafranceschina

RECOMMENDED:

David E. Newman, Ph.D.

Curt A. L. Szuberla, Ph.D.

Renate Wackerbauer, Ph.D.
Advisory Committee Chair

Curt A. L. Szuberla, Ph.D.
Chair, Department of Physics

APPROVED:

Paul W. Layer, Ph.D.
Dean, College of Natural Science and Mathematics

John C. Eichelberger, Ph.D.
Dean of the Graduate School

4/25/14

Date

TRANSIENT SPATIOTEMPORAL CHAOS IN A DIFFUSIVELY AND SYNAPTICALLY COUPLED MORRIS-LECAR NEURONAL NETWORK

A

THESIS

Presented to the Faculty

of the University of Alaska Fairbanks

in Partial Fulfillment of the Requirements

for the Degree of

MASTER OF SCIENCE

By

Jacopo Lafranceschina, B.S. Physics

Fairbanks, Alaska

May 2014

Abstract

Transient spatiotemporal chaos was reported in models for chemical reactions and in experiments for turbulence in shear flow. This study shows that transient spatiotemporal chaos also exists in a diffusively coupled Morris-Lecar (ML) neuronal network, with a collapse to either a global rest state or to a state of pulse propagation. Adding synaptic coupling to this network reduces the average lifetime of spatiotemporal chaos for small to intermediate coupling strengths and almost all numbers of synapses. For large coupling strengths, close to the threshold of excitation, the average lifetime increases beyond the value for only diffusive coupling, and the collapse to the rest state dominates over the collapse to a traveling pulse state. The regime of spatiotemporal chaos is characterized by a slightly increasing Lyapunov exponent and degree of phase coherence as the number of synaptic links increases. In contrast to the diffusive network, the pulse solution must not be asymptotic in the presence of synapses. The fact that chaos could be transient in higher dimensional systems, such as the one being explored in this study, point to its pres-ence in every day life. Transient spatiotemporal chaos in a network of coupled neurons and the associated chaotic saddle provide a possibility for switching between metastable states observed in information processing and brain function. Such transient dynamics have been observed experimentally by Mazor, when stimulating projection neurons in the locust antennal lobe with different odors.

Table of Contents

List of Figures

Page

List of Tables

Page

Acknowledgements

I would like to express my appreciation and thanks to my advisor Dr. Renate Wackerbauer, for introducing me to such fascinating subject, for her motivation, guidance and encouragement given throughout the development of this work. I would like to thank my committee members, Dr. David E. Newman and Dr. Curt A. L. Szuberla, for the suggestions and helpful tips they provided. I would like to acknowledge the Physics Department at the University of Alaska Fairbanks, for the funding of this work, and the Alaska Satellite Facility for the additional funding provided. I would also like to acknowledge the Arctic Region Supercomputing Center for the use of their machines, and the Graduate School at the University of Alaska Fairbanks for the travel grant given me to present my research at the American Physical Society 2014 March Meeting. Furthermore I would also like to acknowledge my colleagues Douglas Ogata and Mark Graybill for their helpful hints. Last but not least, a special thanks goes to my wife Rachel and my two kids, Brooklyn and Giuseppe, for their patience and understanding through the long days spent doing research.

Chapter 1
Introduction

Transient chaos is a special case of chaotic dynamics in which the system dynamics spontaneously collapses to a system attractor without external perturbation. Such collapse is typically associated with the existence of a chaotic saddle[1], i.e., an invariant manifold that is not attractive. Recent studies in Neuroscience suggest that a good candidate for the switching of neural activity between metastable states could be due to a sequence of saddle points[2]. We argue that chaotic saddles might be important in this context since they allow for more complex dynamics near a metastable state.

Transient chaos has been reported for several systems and across scientific disciplines. Transient chaos in low-dimensional dynamical systems has been studied, e.g., in a three species food chain model for species extinction in ecology[3], and in Chua's electronic circuits[4]. *Transient spatiotemporal chaos* has been found in reaction-diffusion models for semiconductor charge transport[5], for the CO oxidation on a single-crystal Pt surface[6], for a cubic autocatalytic reaction[7], and for turbulence in shear flows[8]. Recently, transient spatiotemporal chaotic dynamics has been shown to exist in a ring network of diffusively coupled, identical Morris-Lecar[9] (ML) neurons[10].

In a realistic neural network the main connections are electrical and chemical synapses. Chemical synapses involve the release of a neurotransmitter that either inhibits or excites the postsynaptic neuron. An electric synapse is a much shorter, faster and simpler connection happening through gap junctions between neighboring neurons via diffusive coupling. Models for neuron networks often focus on synaptic coupling. The importance of diffusive coupling in model systems has recently been linked to the observed lateral potassium diffusion in neuronal networks[11]. In an ML network, diffusively and synaptically coupled, chemical synapses have been shown to be more efficient in enhancing stochastic coherence[12].

This study explores transient spatiotemporal chaos when synapses are added to a diffusively coupled ML neuronal ring network. The synapses are modeled as excitatory, chemical synaptic coupling that activate AMPA receptors for glutamate. This particular receptor is commonly used in network models [13], and has a fast excitatory response. The model is introduced in Chapter 2. Statistics and dynamical properties of transient chaos in the presence of synapses are presented in Chapter 3. Chapter 4 discusses the possibility of chaos initiation upon collapse.

Chapter 2
Model

A network of N diffusively and synaptically coupled, identical, excitatory Morris-Lecar neurons is considered[9, 14] (Fig. 2.1a). The membrane potential V_i, and the fraction of open potassium channels n_i for neuron i is modeled by

$$\dot{V}_i = \frac{1}{C_m}(-I^{ion} - I^{syn} + I) + D\Delta_i, \tag{2.1}$$

$$\dot{n}_i = \tau_n (n_{ss} - n_i), \tag{2.2}$$

where C_m is the membrane capacitance per unit area, I^{ion} is the ionic current, I^{syn} is the synaptic current and I is the applied current. When I^{syn} is set to zero the network is only diffusively coupled. The Δ operator characterizes the diffusive coupling between neighboring neurons, defined as $\Delta_i = (V_{i-1} + V_{i+1} - 2V_i)$. D is the diffusive coupling strength. The ionic current, I^{ion}, models the membrane activity as the sum of three ohmic currents: the inward calcium current, the outward potassium current, and the leak current associated with other ion fluxes.

$$I^{ion} = g_{Ca} m_{ss}(V_i - V_{Ca}) + g_K n_i (V_i - V_K) + g_L (V_i - V_L). \tag{2.3}$$

The open-state probability functions, m_{ss} and n_{ss}, and the term τ_n are associated with the time course of potassium channel activation. These terms are governed by

$$m_{ss} = \frac{1}{2}\left(1 + \tanh\left[\frac{V_i - V_1}{V_2}\right]\right), \tag{2.4}$$

$$n_{ss} = \frac{1}{2}\left(1 + \tanh\left[\frac{V_i - V_3}{V_4}\right]\right), \tag{2.5}$$

$$\tau_n = \varphi \cosh\left(\frac{V_i - V_3}{2V_4}\right). \tag{2.6}$$

The parameters used in the above equations are summarized in Table I. The synaptic current in Eq. (2.1) is also modeled as an ohmic current[15],

$$I^{syn} = g\sum_{j=1}^{N} w_{j,i} s_{j,i}(V_i - V_s), \tag{2.7}$$

Table 2.1. Model parameters for the Morris-Lecar (Type I) neuron[9, 14] and for synaptic coupling with AMPA receptor[16]

C_m	Membrane Capacitance	20 μF/cm^2
g_K	Potassium Conductance	8 mS/cm^2
g_L	Leak Conductance	2 mS/cm^2
g_{Ca}	Calcium Conductance	4 mS/cm^2
V_K	Potassium Equilibrium Potential	-80 mV
V_{Ca}	Calcium Equilibrium Potential	120 mV
V_L	Leak Equilibrium Potential	-60 mV
V_1	Calcium Activation Potential	-1.2 mV
V_2	Fitting parameter for Voltage	18 mV
V_3	Potassium Activation Potential	14.95 mV
V_4	Fitting Parameter for Voltage	17.4 mV
φ	Inverse Time Scale for Recovery Process	1/15 s
V_s	Reversal Potential of the Channel	0 mV
α	Growth Rate of Synaptic Conductance	1.1 $mM^{-1}ms^{-1}$
β	Decay Rate of Synaptic Conductance	0.19 ms^{-1}
T_m	Maximal Concentration of Transmitter	1.0 mM
V_p	Voltage for Half-maximal Rate	2.0 mV
K_p	Steepness of the Voltage Dependence	5.0 mV

where g is the conductance of the synapse, $w_{j,i}$ represents the synaptic coupling matrix with $w_{j,i}$=1, if there exists a synaptic link from neuron j to i, otherwise $w_{j,i}$=0. $s_{j,i}$ is the fraction of open channels in the synaptic link between neuron j and i, and V_s is the reversal potential of the channel. The fraction of open channels is modeled by

$$\dot{s}_{j,i} = \alpha T(1 - s_{j,i}) - \beta s_{j,i}, \tag{2.8}$$

where T is the concentration of the neurotransmitter in the synaptic cleft, α and β are rise and decay time constants respectively. The concentration of neurotransmitter T depends on the membrane voltage of the presynaptic neuron V_j, and is modeled by a sigmoidal function,

$$T = \frac{T_m}{1 + exp\left(-\frac{(V_j - V_p)}{K_p}\right)}. \tag{2.9}$$

where T_m, V_p, and K_p represent parameter values defined in Table I. Figure 2.1b shows how the fraction of open channels changes in time subject to different presynaptic membrane potentials starting with three representative initial values for s.

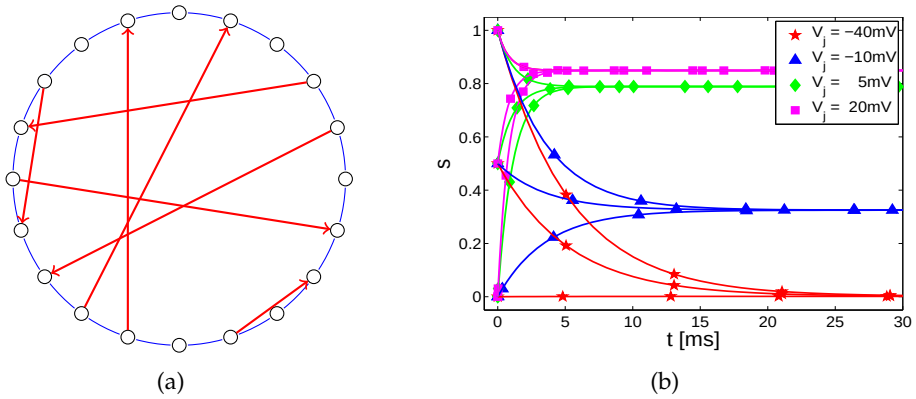

Figure 2.1. Network topology and time evolution of the fraction of open channels. (a) Example network topology for a ring network of N=20 diffusively coupled identical ML neurons, with the addition of N_s=7 (unidirectional) synaptic links (red arrows). (b) Typical time evolution of the fraction of open channels (s) for several presynaptic membrane potentials V_j and initial conditions $s(t=0)$=0, 0.5, 1.0.

A bifurcation analysis for the single Morris-Lecar neuron shows that the neuron[10, 14] is excitable below I=38.7$\mu A/cm^2$, where the SNIC (saddle-node on invariant circle) bifurcation occurs. In this excitable regime the system has three steady states, a stable node, a saddle point, and an unstable focus. A typical excitation cycle for a single ML neuron is shown in Fig. 2.2. If a neuron gets perturbed above a critical threshold, the trajectory goes around the unstable focus to then return to the stable node. Above I=38.7$\mu A/cm^2$ the system presents a stable limit cycle and thus oscillatory behavior. At the subcritical Hopf bifurcation near I=41.4$\mu A/cm^2$, the unstable focus becomes stable and an unstable limit cycle is born. The threshold for excitation in an ML ring network is near I=28$\mu A/cm^2$. Throughout this study an intermediate value in the excitable regime, I=32$\mu A/cm^2$, was used.

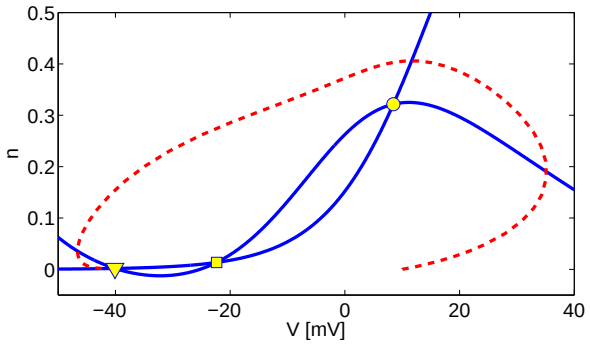

Figure 2.2. A typical excitation cycle in phase space (red, dashed line) for a single Morris Lecar neuron (I=32$\mu A/cm^2$). The two nullclines (blue) and the three steady states, a stable node (triangle), a saddle point (square), and an unstable focus (circle) are shown.

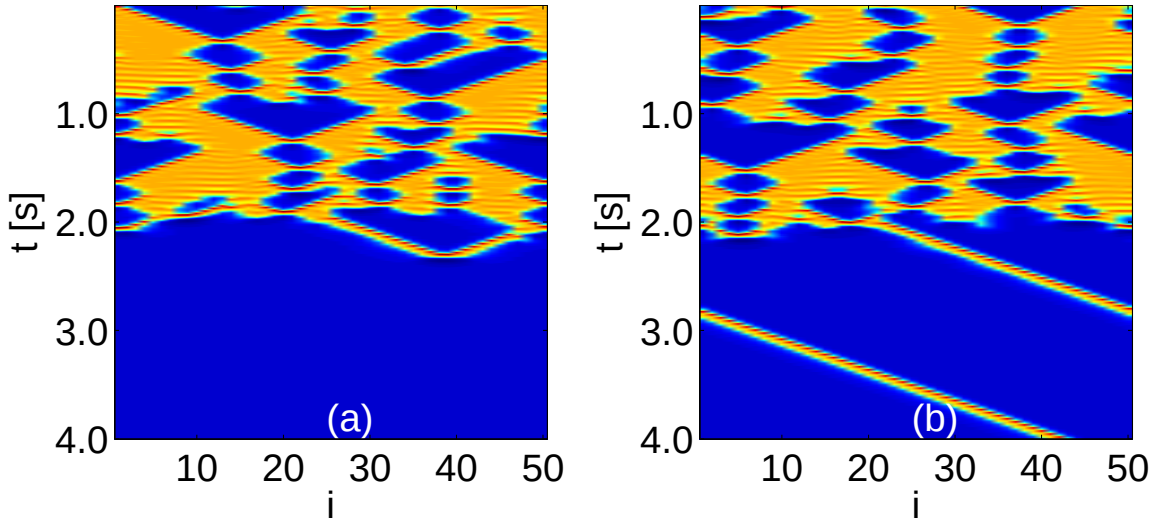

Figure 2.3. Collapse of transient spatiotemporal chaos in a diffusively coupled ML network of size N=50. a) Collapse to a global rest state. b) Collapse to a traveling pulse solution. The colors indicate a membrane potential value close to the unstable focus (orange) or close to the stable point (blue).

In a diffusively coupled ML ring network the spatiotemporal chaos is transient[10]. The network remains in the chaotic state until a sudden collapse to either the rest state (stable node) or a pulse solution (Fig. 2.3). The rest state corresponds to a global steady state where every neuron in the network is at the stable node. The pulse solution is associated with the network reaching a homoclinic orbit in phase space. Two distinct pulses have been observed, a wide pulse and a narrow pulse. They differ in their pulse profile (Fig. 2.4a), in their phase portraits (Fig. 2.4b), and in their spatiotemporal representation (Fig. 2.4c,d). Another important aspect of a diffusively coupled ML ring network is that the average lifetime of the chaotic transient increases exponentially with the network size. This study explores how all of those characteristics change when synaptic links are added to the diffusive network.

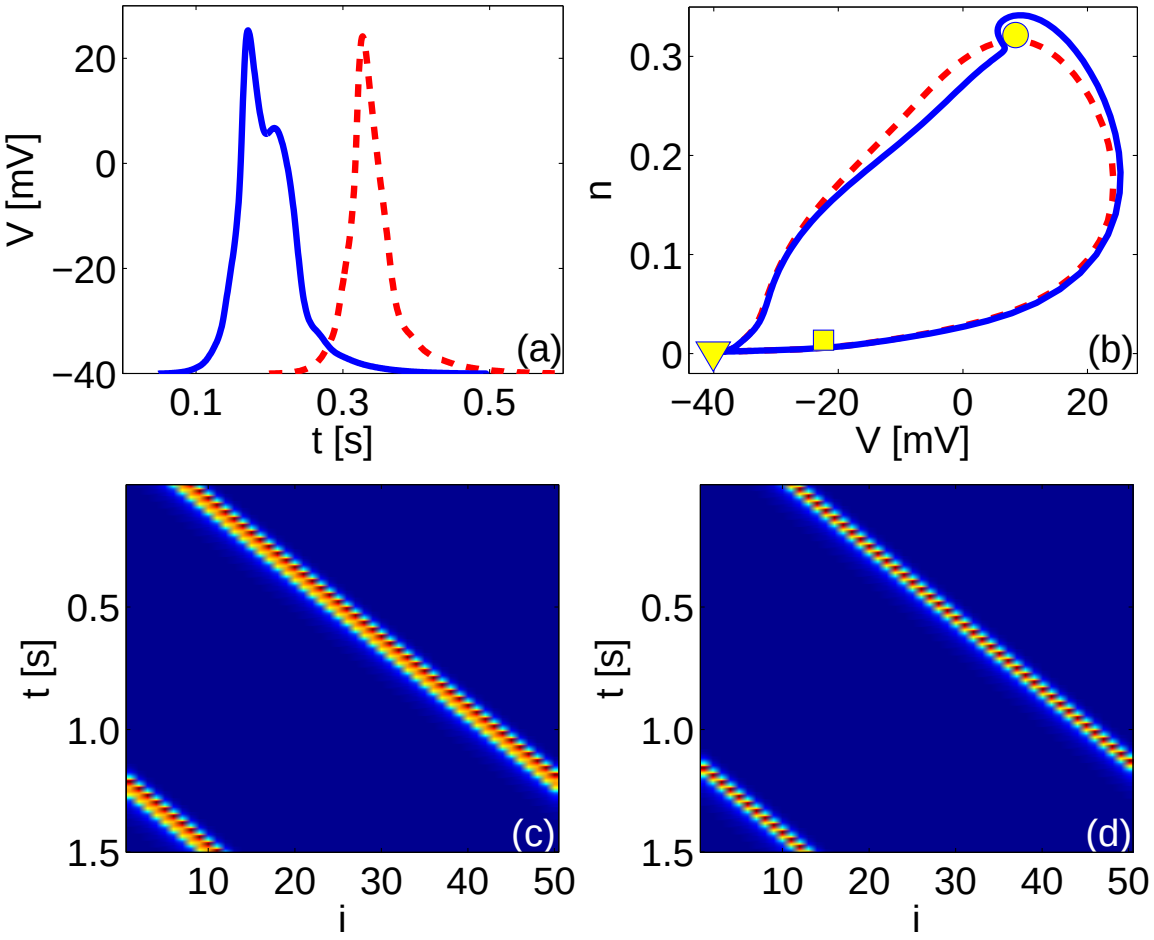

Figure 2.4. Comparison between wide and narrow pulse. Comparison of membrane potential V between narrow (dashed line) and wide (solid line) pulse solutions. a) Time evolution of the pulses, (b) phase portrait, and spacetime pattern for the wide (c) and the narrow (d) pulse solution.

Chapter 3
Adding synaptic coupling

A variety of synaptic links are added to the diffusively coupled ML ring network. The synaptic links are unidirectional and restricted to no more than one per neuron. The number of synaptic links, N_s, the length of a synaptic link, L_s, and the coupling strength, g, are the main parameters. Typical spacetime patterns of a synaptically coupled neural network are shown in Fig. 3.1. States of excitation (orange) are alternated with states where neighboring neurons are close to the rest state (blue). For low enough coupling strength, g=0.3mS/cm^2, the spatiotemporal patterns are similar to the diffusive case, and independent on the number of links. As the coupling strength g increases (g=1.0 mS/cm^2) the spatiotemporal pattern starts to change for high N_s. Larger regions of neurons in the rest state become more rare. The timescale of neighboring neurons in the rest state decreases. For g=1.7mS/cm^2 and g=2.4mS/cm^2 this behavior becomes more extreme. For a high number of synaptic links, the active and non-active regimes become more localized. The "diffusive neighborhood" is destroyed by the nonlocal synaptic couplings, thus creating the vertical patterns in Fig. 3.1. The critical coupling strength above which a single synapse from an active presynaptic neuron can excite a postsynaptic neuron is g=2.5mS/cm^2.

The neurons' phase coherence is measured with the Kuramoto [17] order parameter. The amplitude R$\in$[0,1] of the mean field neuron population is given by

$$Re^{i\psi} = \frac{1}{N}\sum_{j=1}^{N} e^{i\theta_j}, \tag{3.1}$$

where θ_j is the phase of neuron j relative to the unstable focus, and ψ is the mean field phase. When a network undergoes the collapse of the chaotic state to the global rest state, the order parameter will reach its maximum value, R=1 (Fig. 3.2a, b). For a collapse to a pulse solution, R will oscillates below one within a small amplitude (Fig. 3.2b). The order parameter was measured for a network of N=100 neurons with $N_s \in [1, N/2]$ links at three representative values of g. A sample illustrating the convergence behavior of R is shown in Fig. 3.3a. The phase coherence R for small coupling strength, g=0.3mS/cm^2, is much lower than for the cases where g=1.0mS/cm^2 or g=1.7mS/cm^2. For each coupling strength there are a total of 100 simulations with a combination of 10 initial conditions for V and n, and 10 random link locations. For every simulation the time it takes to reach convergence of the order parameter was short.

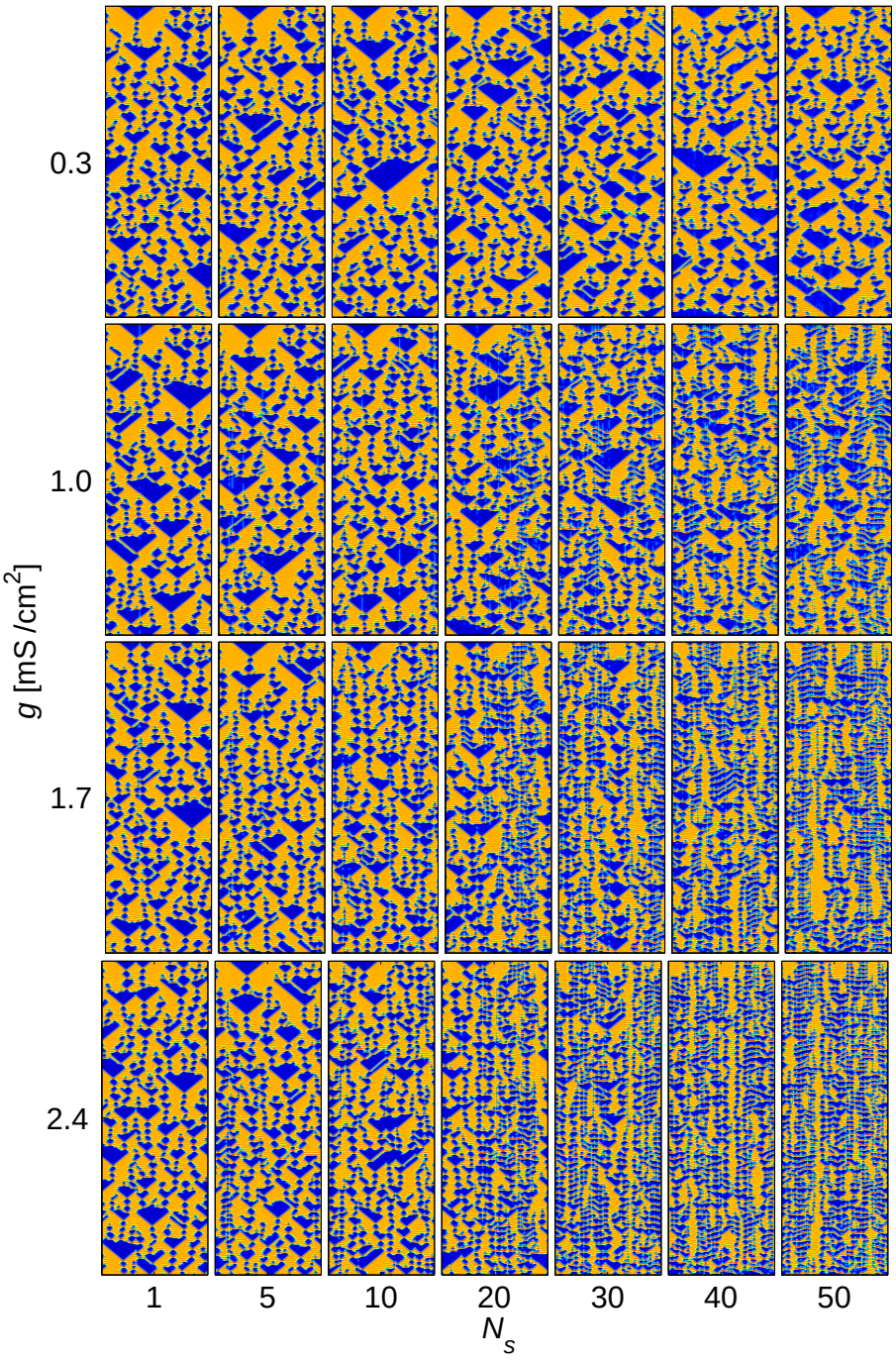

Figure 3.1. Spatiotemporal dynamics in the presence of synaptic links. Spatiotemporal dynamics for the membrane potential (V) in a ring network of N=100 diffusively coupled Morris-Lecar neurons to which N_s synaptic links have been added with varying coupling strength g. The length of each link is randomly chosen, with the constraint that any neuron can only be part of a single synapse. Colors indicate when the membrane potential is close to the resting potential (blue) or close to the unstable focus (orange). Each simulation has been started with the same initial chaotic state, and the synaptic coupling was added at time t=0. Each of the spatiotemporal patterns is analogous to Fig. 2.3, covering a time interval of 10 s and 100 neurons.

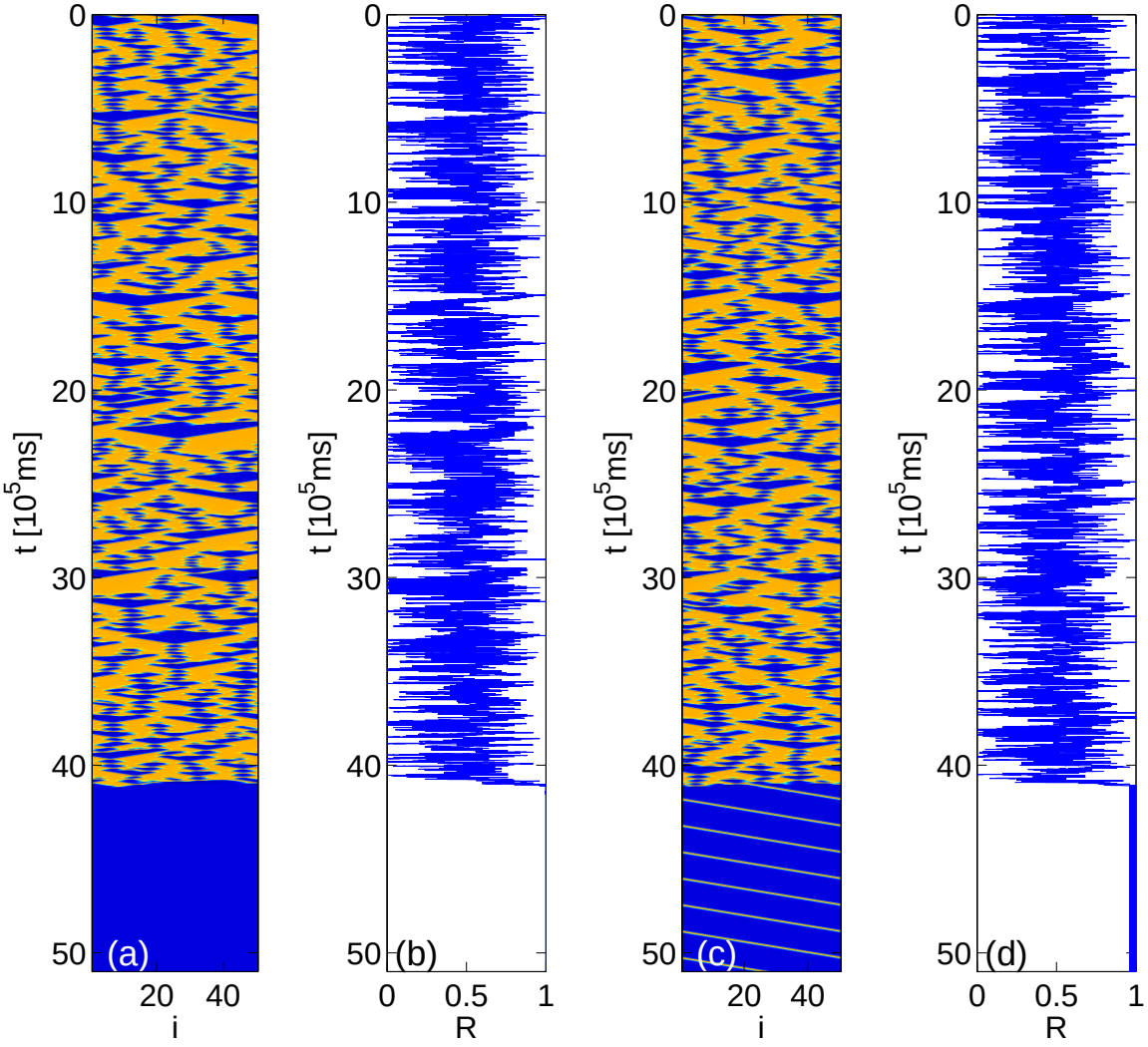

Figure 3.2. Spatiotemporal dynamics and corresponding order parameter, R, for a diffusively coupled ML network of N=50 neurons, for the collapse of chaos to (a, b) the global rest state, and to (c, d) a pulse solution.

For small coupling strength (g=0.3mS/cm^2), the average order parameter, $\langle R \rangle$, is slightly increased in comparison to the diffusively coupled network, independent of the number of synapses, N_s (Fig. 3.3b). This behavior is consistent with Fig. 3.1; the spatiotemporal patterns, for high N_s are statistically indistinguishable from a network that is just diffusively coupled. For intermediate coupling strength, g=1.0mS/cm^2, $\langle R \rangle$ increases almost linearly with N_s, until N_s=30 where it seems to reach a plateau. For, g=1.7mS/cm^2, $\langle R \rangle$ increases with increasing N_s, and does not reach a plateau even for the largest possible number of synapses.

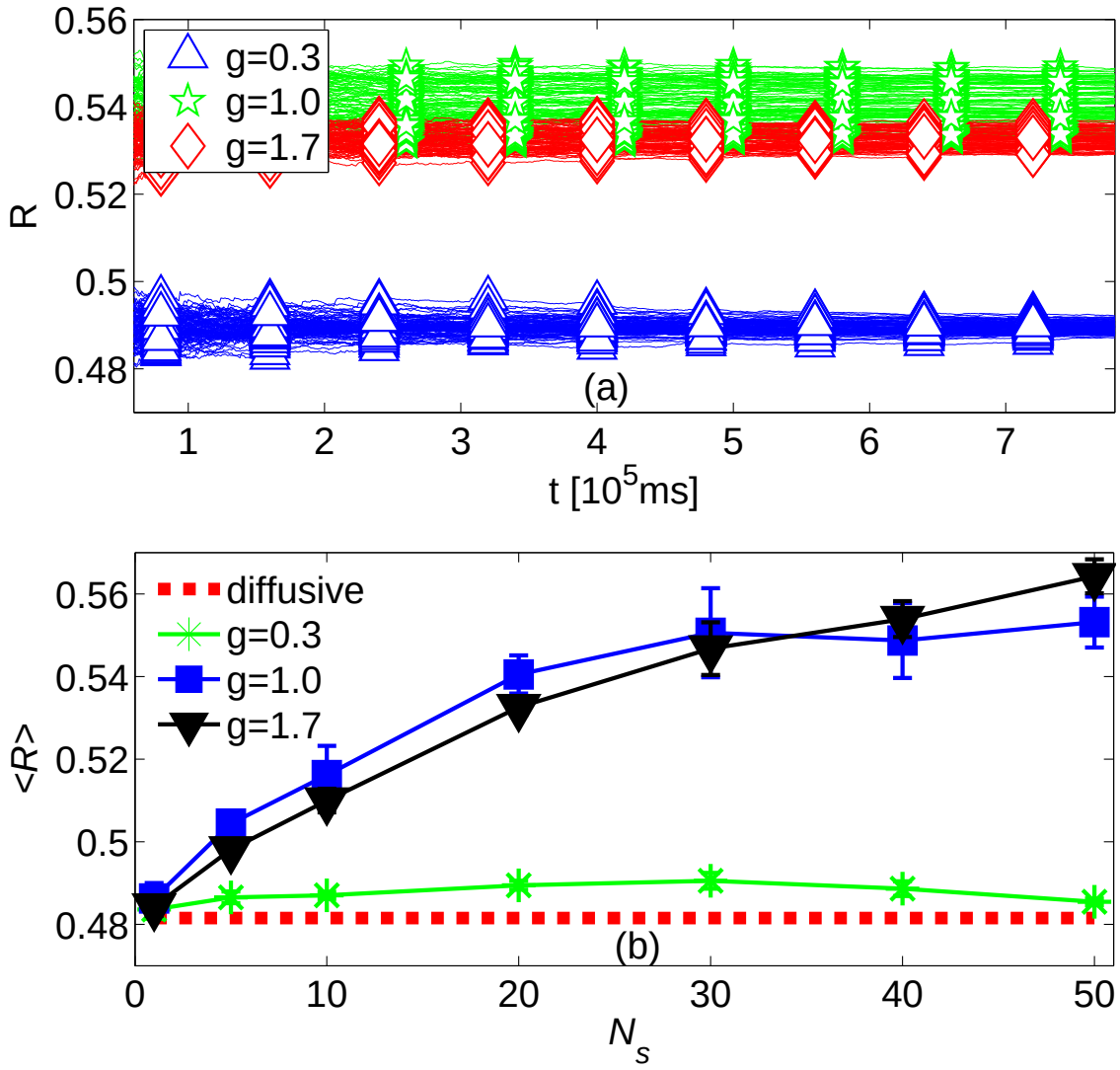

Figure 3.3. Convergence behavior of the order parameter. (a) Convergence behavior of the order parameter, R, for an ML network with N=100 neurons, and N_s=20 synaptic links of strength g=0.3 mS/cm^2 (blue), g=1.0mS/cm^2(red), and g=1.7mS/cm^2(black). For each coupling strength there are a total of 100 simulations with a combination of 10 initial conditions for V and n, and 10 random locations for N_s links. (b) The average order parameter, $\langle R \rangle$, versus the number of synapses, N_s, for different coupling strength, g. The statistical analysis of transient chaos is done on a network of size N=100 to ensure a long enough lifetime to reach convergence.

Figure 3.4 shows the order parameter, R, for a wide variety of coupling strengths and number of links, covering the entire range of possible link numbers and also coupling strengths for up to the critical coupling strength where a synapse induces excitation. For a single synaptic link, N_s=1, the order parameter, R, is close to the order parameter for the diffusive case for all coupling strengths. For larger number of couplings, N_s, the order

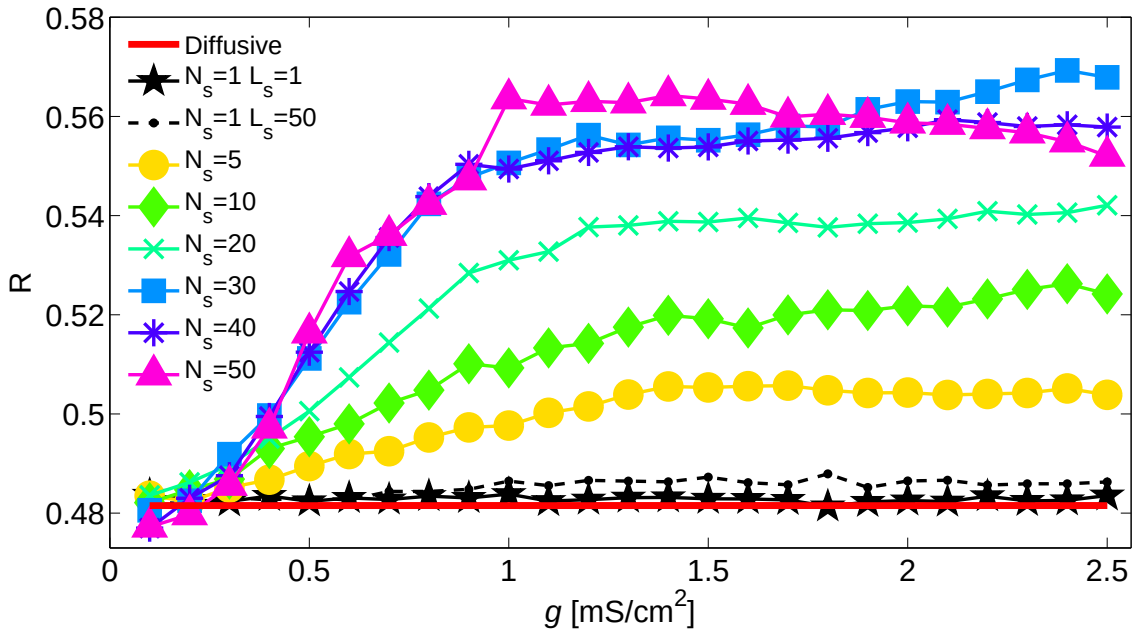

Figure 3.4. Order parameter versus coupling strength. Order parameter, R, versus coupling strength for transient chaos on an ML network with N=100 neurons. Each line represents a different number of synaptic links, N_s. The location of the synaptic link was chosen randomly. For N_s=1 a link length of L_s=1 and L_s=$N/2$ are shown; for all others, L_s was randomly chosen.

parameter starts out the same as for the diffusive case, then increases clearly with increasing coupling, until it levels off, typically remaining close to constant. For a network with maximum possible number of links, N_s=$N/2$, R increases until g=1mS/cm^2 where it starts to decrease. From the order parameter study it can be deducted that a single synaptic link, or a high number of links at low coupling strength, do not change the dynamics (phase coherence) on the network. On the other hand, as g increases the effects on the dynamics are visible and distinct for every N_s case, resulting in an increase in the averaged order parameter.

The convergence behavior of the finite time Lyapunov exponent[18] shows that the spatiotemporal dynamics is chaotic in the presence of synapses. The Lyapunov exponent, λ, convergences to a positive value that is different from the diffusive case, implying that synapses influence the strength of chaos for a variety of coupling strengths. An example for convergence of the largest Lyapunov exponent for a network with an intermediate number of synaptic links, N_s=20, at several coupling strengths, is given in Fig. 3.5a. The dynamics is typically more chaotic than without a synapse and the error bar increases with increasing coupling strength, g. For high coupling strength above the critical coupling

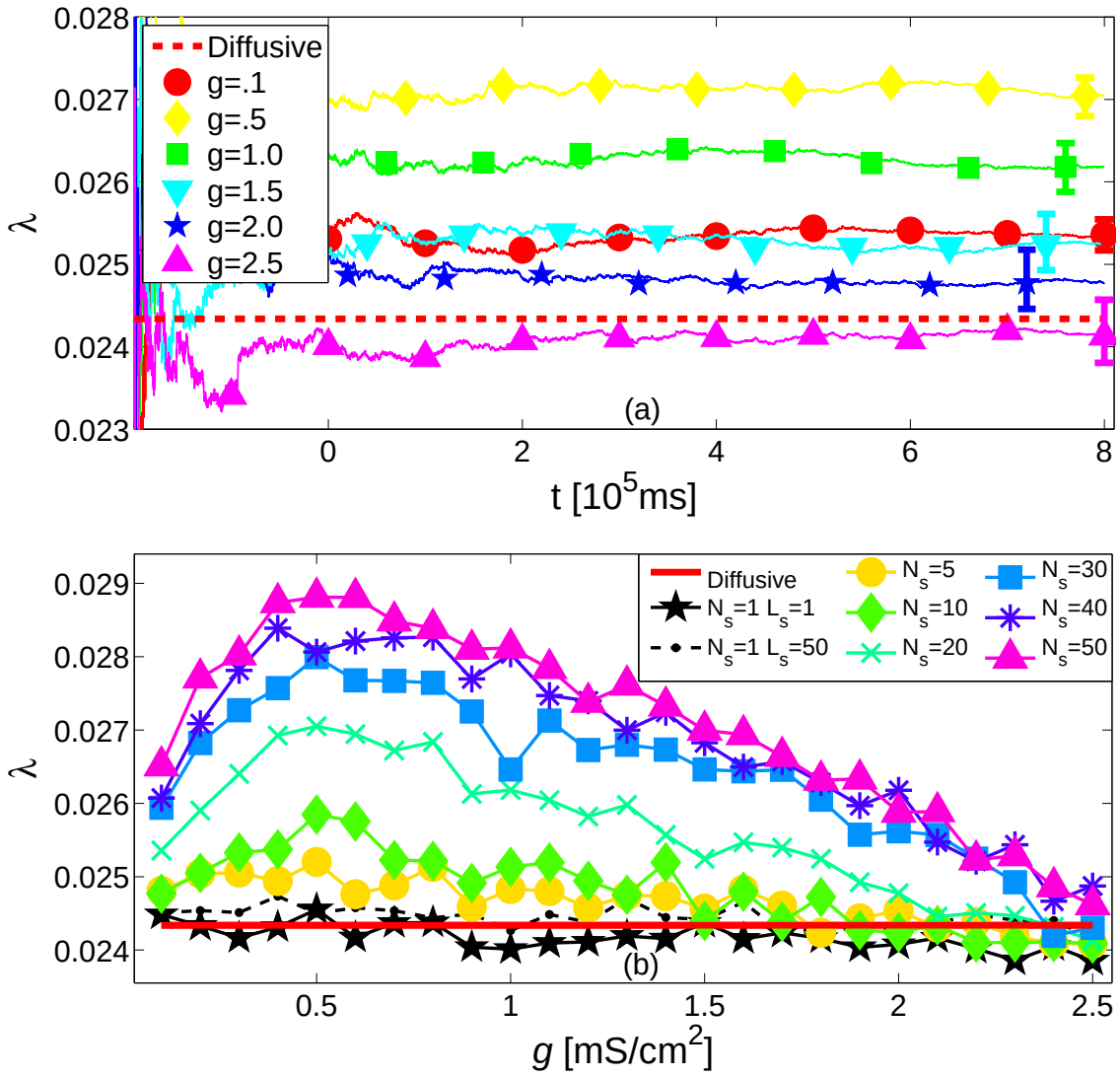

Figure 3.5. Lyapunov exponent convergence and dependence on the coupling strength. (a) Convergence behavior of the largest Lyapunov exponent, λ, in an ML network of N=100 neurons and N_s=20 synapses, at several coupling strengths g. The error bar was calculated from 100 simulations, a combination of 10 random initialization of V and n, and 10 random locations of links. The error bars are offset in the figure for a more clear representation. (b) Lyapunov exponent for an ML network of N=100 neurons, where convergence is reached in good approximation. Each line represents a different number of synaptic links, N_s. The location of the synaptic link was chosen randomly. For N_s=1 a link length of L_s=1 and L_s=$N/2$ are shown. The diffusive case is shown as a dotted line.

strength of synapse-induced excitation, the dynamics is slightly less chaotic than for the diffusive case. The Lyapunov exponent is shown in Fig. 3.5b for several g and N_s values. For few links, N_s=5, the Lyapunov exponent is slightly above the value of the diffusive case. As N_s increases further, λ differs more and more from the diffusive case. λ increases (faster) for low g, and then after reaching its maximum value at around g=0.5mS/cm^2, it

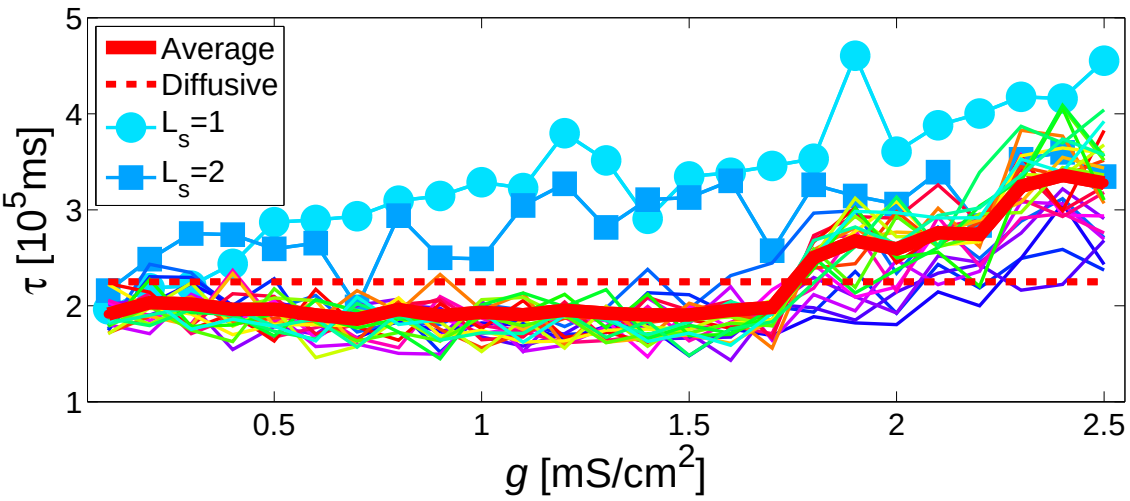

Figure 3.6. Lifetime of transient chaos for single synapse. Lifetime of transient chaos, τ, versus coupling strength, g for a network with N=50 neurons with a single synapse, N_s=1, at different length, L_s=1,..,25. Each line represents a L_s. The bold red line shows the average over all L_s. The chaotic initial condition is the same for all simulations.

decreases reaching the λ for the diffusive case for large coupling strengths (g=2.5mS/cm^2).

After the chaotic phase the network dynamics collapses to either a rest state or a pulse solution. The time the network requires to reach the collapse of the chaotic state is called lifetime. The lifetime, τ, was first calculated for a network where only a single synaptic link of length L_s was introduced (Fig. 3.6). For small links L_s=1 and L_s=2, τ is increasing with increasing coupling strength g, and usually greater than the average lifetime for the diffusive case. For any other L_s, the collapse is reached faster than for the diffusive case, for small and intermediate coupling strength (up until g=1.7mS/cm^2). For large coupling strength, τ starts increasing rapidly with increasing coupling strength. For N_s=5 the average lifetime for 100 collapses (Fig. 3.7), is close to the average value for a single synaptic link (Fig. 3.6). As more links are added to the network; the effects on the lifetime are more noticeable. The average lifetime at first decreases below the value for the diffusive case for low g. As the coupling strength increases to intermediate and high values, g>1mS/cm^2, $\langle\tau\rangle$ increases. Around g=1.6mS/cm^2, $\langle\tau\rangle$ passes the value for the diffusive network, and clearly increases with g. The longest average lifetime was obtained when the network was coupled with an intermediate value of N_s=15 links.

Figures 3.6 and 3.7 reveal that a single synaptic link can influence the lifetime of a diffusively coupled network. A short, single link increases the lifetime of the network, while

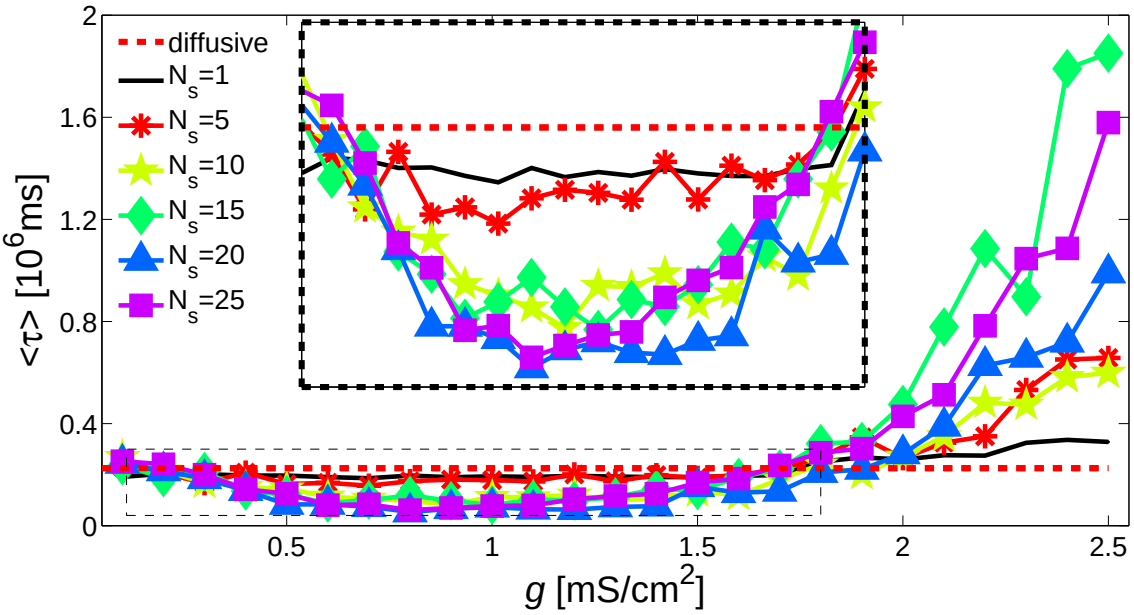

Figure 3.7. Mean lifetime versus coupling strength. Mean Lifetime, $\langle\tau\rangle$, versus coupling strength, g, for a network with N=50 neurons and different number of synapses, N_s. Each colored line represents a given number of synaptic links. Each point of a line is an average over 100 simulations combined from 10 random initial (V,n) conditions and 10 random synaptic link locations. For a single synaptic link, the average was done over all possible link lengths L_s=1,..,25, and a single chaotic initial condition, and a single location of synapse. Inset shows a zoom in of the boxed region.

a link length longer than two neurons decreases the lifetime to even shorter times than for the diffusive case, unless the coupling strength is high enough to overcome the threshold of excitability. When the network is coupled with more synaptic links at a low coupling strength g, the order parameter (Fig. 3.4) and the spatiotemporal patterns (Fig. 3.1) are similar to the diffusive case while the Lyapunov exponent increases for increasing number of synapses, and the transient lifetime decreases to even shorter values than for the diffusive case. On the other hand for large coupling (g>$1mS/cm^2$), the order parameter increases, the Lyapunov exponent decreases, the spatiotemporal pattern exhibits different features from the diffusive case, and the lifetime of the transient chaos increases with increasing g.

The addition of synaptic links also influences the state that is reached upon collapse. Once the network is synaptically coupled, the percentage of pulse solutions is typically less than in the diffusive case. Figure 3.8 shows the frequency of collapse to a pulse solution (P) for various coupling strengths g, and number of links, N_s. Without synaptic coupling, about 50% of the 100 simulations reach a pulse state, and not the rest state. For a single synaptic link the percentage of pulse solutions, P, fluctuates between 40-50% for low and

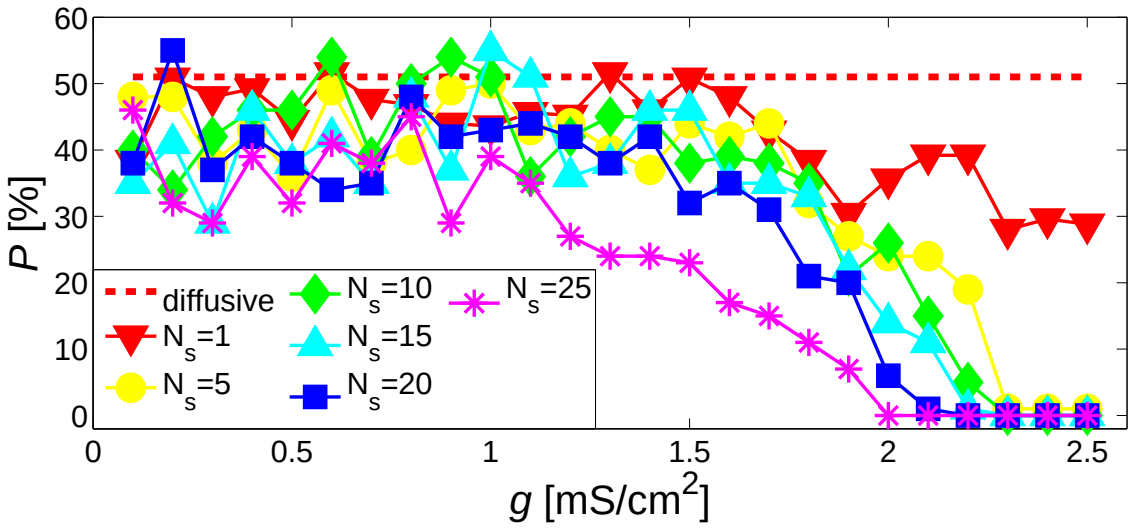

Figure 3.8. Percentage of collapse to a pulse solution. Percentage P of collapse to a pulse solution for a network with N=50 neurons at different coupling strength, g, and number of synaptic links, N_s. The dashed line shows the diffusive case.

intermediate values of coupling strength. For higher values of g, the percentage of pulse solutions starts decreasing, reaching a value of 30%. As N_s increases, this trend is repeated, showing that P starts to decrease at even lower values of g, reaching a value of P=0 for high g. With more synapses the network collapses only to the rest state for sufficiently large coupling strength. The decrease of P for increasing g is qualitatively understandable; in this case the lifetime of transient chaos is large, and the asymptotic state will be less likely a pulse solution, in agreement with Fig. 3.7. This behavior shows that the collapse to the pulse state is avoided for high coupling strength, because the synaptic links prevent the collapse to pulse by providing super threshold perturbations to further excite the system.

Chapter 4
Chaos initiation after collapse

After the collapse of the chaotic state, the network is in a state of global rest or it will have collapsed to a traveling pulse solution. In a network that has only diffusive couplings, these two states are permanent unless being perturbed by an external source (Fig. 4.1a). On the other hand, when a network is both diffusively and synaptically coupled, the chaos state can be initiated from a pulse solution under particular conditions (Fig. 4.1b). Such behavior happens even when the synaptic coupling strength is very low. A synaptically coupled network that collapses to a wide pulse can shift to a narrow pulse solution before initiating chaos. The location of the change from wide pulse to narrow pulse, and the location of the start of chaos is near the location of the postsynaptic neuron (Figs. 4.1 c, d).

To better understand the conditions for chaos onset, *a single pulse in the presence of a single synapse* is studied for varying coupling strength and link length, and representative spacetime patterns are shown in Fig. 4.2. Depending on the parameters an initially wide pulse solution can be either asymptotic, or initiate chaos during its first interaction with the synaptic coupling, or it can become a narrow pulse during its first interaction with the synapse. The narrow pulse can then be either asymptotic or initiate chaos after its first interaction with the synapse. Figure 4.3a shows a binary map of the system state (for a wider range of parameters than Fig. 4.2) in the parameter space, given by the strength and length of the synapse. An asymptotic pulse solution is labeled as black pixel, whereas chaos initiation is labeled as a white pixel. For low coupling strengths chaos initiation happens for link lengths of $L_s \leq 9$ neurons (Fig. 4.3a), indicating that the link connects neurons within the pulse. The shorter the link length, L_s, the lower the coupling strength needs to be to initiate chaos. As L_s increases it takes a higher g to initiate chaos. The alternating pattern of chaos and no chaos shown for small L_s is caused by whether the synapse is connected to the back (L_s increasing going left) or the front (L_s increasing going right) of the traveling pulse. Once the link length becomes large enough ($L_s > 9$) chaos is always initiated at coupling strengths above a critical value $g > 1.8\ mS/cm^2$. For a narrow pulse the critical g is higher ($g > 2.4\ mS/cm^2$), and chaos initiation for low coupling strengths is possible for link lengths up to L_s=7 (Fig. 4.3b). The narrow pulse presents less cases of chaos initiation than the wide pulse. Figure 4.3c additionally labels parameter values for which the wide pulse undergoes a switch to the narrow pulse, as presented in Fig. 4.1c. Such switches are only present for small link lengths, L_s. A shift from the narrow pulse to the wide pulse

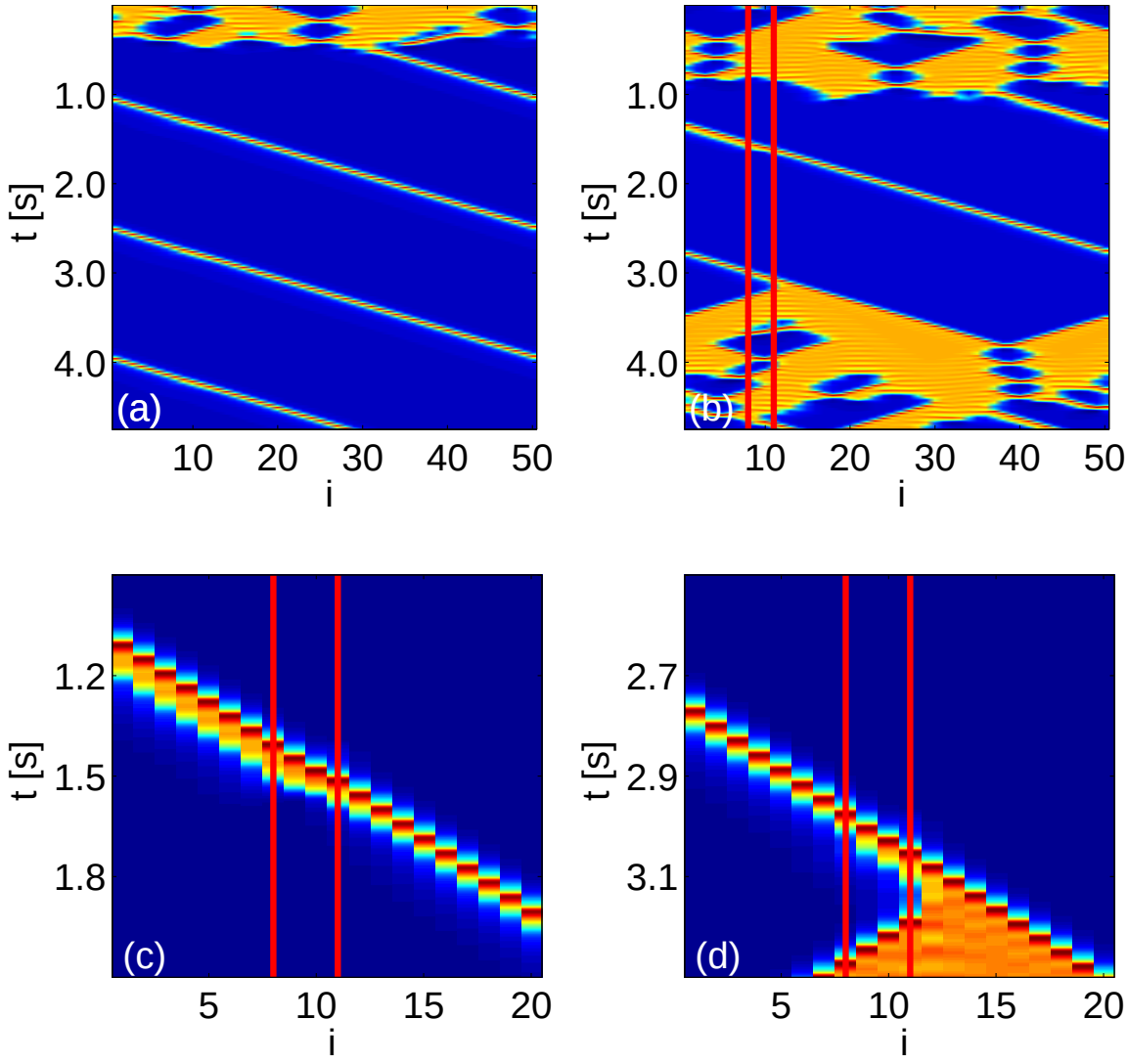

Figure 4.1. Non-asymptotic behavior of synaptic network. (a) Collapse to a pulse solution for a diffusively coupled network (g=0) with N=50 neurons. (b) Onset of chaos after collapse to pulse state in a network with N=50 neurons and a single synapse, from neuron j=8 to i=11 (vertical red lines). Zoom in of Fig.(b), where the change from wide to narrow pulse takes place (c), and where chaos is initiated again (d).

was not observed in the presence of a single pulse. A comparison of the parameters for chaos initiation for the wide and narrow pulse in the map of Fig. 4.3d reveals that the area representing links to the front of the traveling pulse (between L_s=3 and L_s=6 on the right of the map) overlaps (Fig. 4.3d, black circles, white squares). This phenomenon is due to the shape of the traveling pulse (Fig. 2.4).

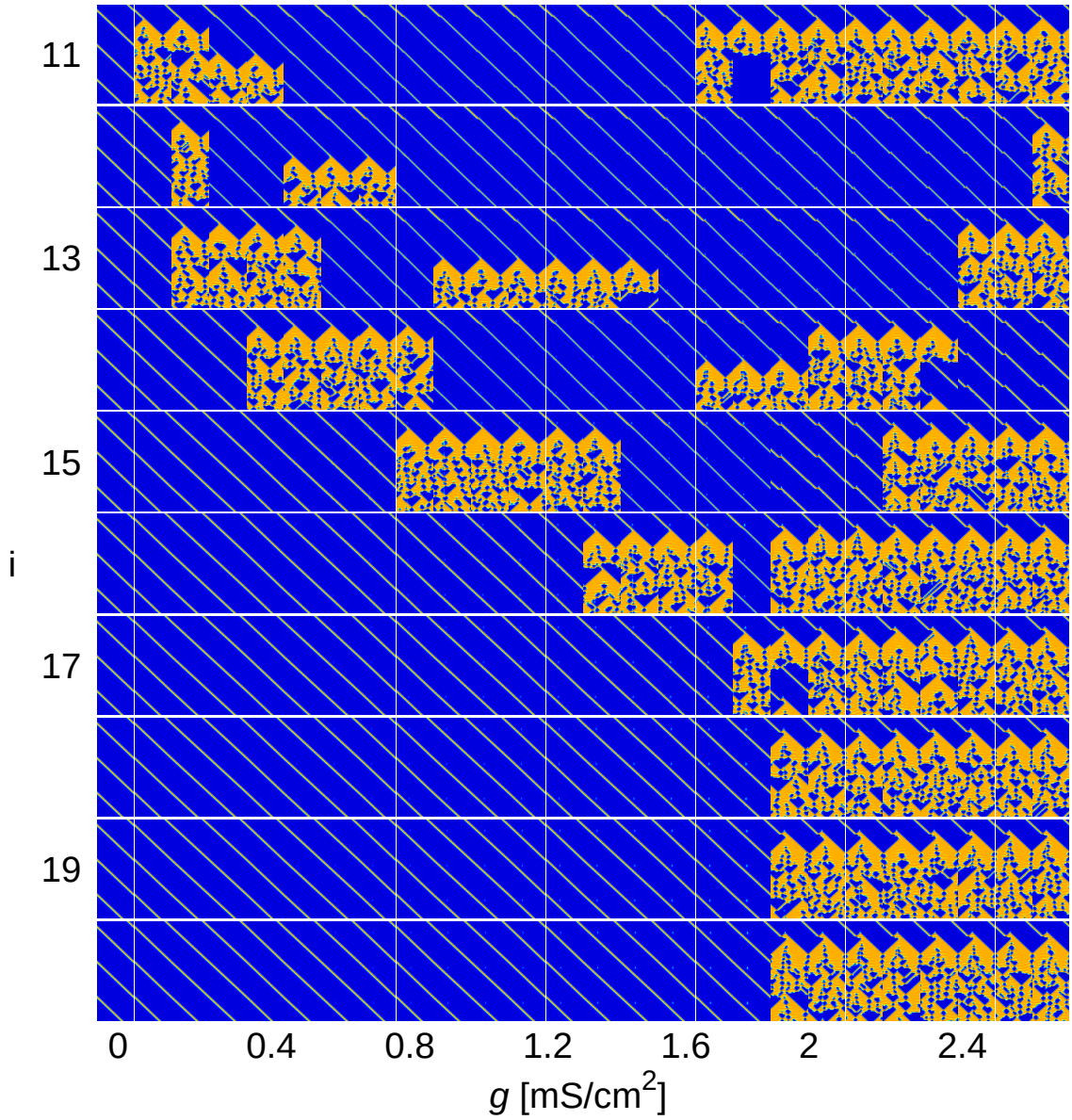

Figure 4.2. Example of chaos initiation. Panel of spatiotemporal evolutions of an initially wide pulse in the presence of a single synaptic link in an ML network of size N=50 neurons, at different coupling strength g and link length. The presynaptic neuron is held constant (j=8), while the link length is varied by changing the postsynaptic neuron (i). The diffusive case corresponds to g=0. For parameter values close to regions of chaos onset, longterm numerical simulations confirm that the pulse stays a pulse. The simulation time for each pattern is 4000*ms*; for other parameters see Fig. 2.3.

A *single pulse in the presence of two synapses* yields more complicated patterns in the maps. For small coupling strengths g, chaos is originated when the postsynaptic neuron i is close to either of the two presynaptic neurons (j=8, and j=33 in this study), such that the synaptic link connects neurons within the pulse near either of the postsynaptic neurons.

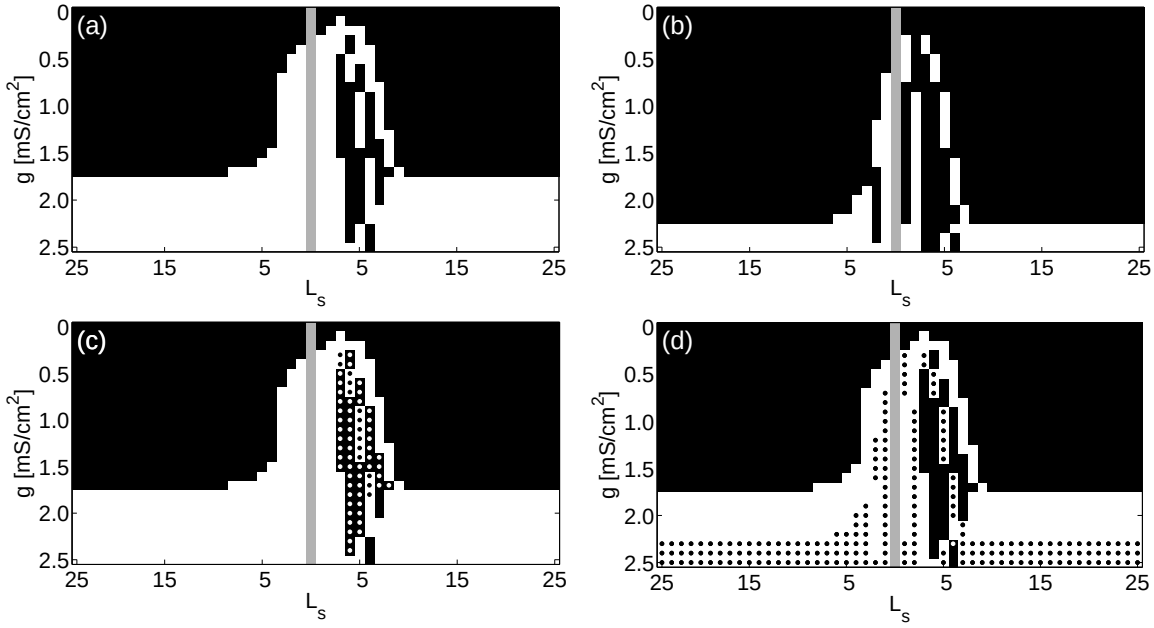

Figure 4.3. Binary map for chaos initiation in the presence of a single synapse. Binary map of the system state for varying coupling strength, g, and length of synapse, L_s, in the presence of a single synaptic link, in analogy to Fig. 4.2. The simulations are started with either a wide pulse (a) or a narrow pulse (b). An asymptotic pulse state is marked with a black pixel, whereas chaos initiation is marked with a white pixel. The map in (c) corresponds to (a), additionally showing the locations where the wide pulse changes to a narrow pulse. The maps in (a) and (b) are superimposed in (d), with dots indicating chaos initiation for the narrow initial pulse.

This causes two "bumps" in the parameter space (Fig. 4.4) that identify chaos initiation for coupling strengths lower than the critical coupling strength. The shape of the bump is related to whether the synapse is connecting the back of the traveling pulse to the front or vice versa. In Fig. 4.4a the front is connected to the back of the right traveling pulse first. As L_{s_8} increases to the left, neuron j=8 is connected first to neurons i=5, 6, and 7 (the back of the traveling pulse) and then to neurons i=9, 10, and 11 as L_{s_8} increases to the right (the front of the pulse). This repeats for neuron j=33, resulting in two almost identical bumps, very similar to the bump for a single synapse. On the other hand when the back of the pulse is connected to the front of the traveling pulse first, the bump will look as reflected (Fig. 4.4b). This happens when neuron j=33 is connected to i=36, 35, and 34 as $L_{s_{33}}$ increases to the right (the front of the traveling pulse) and then to neurons i=32, 31, 30 as $L_{s_{33}}$ increases to the left (the back of the pulse). The small differences in the two bumps are due to the direction of the traveling pulse. For example, the black squares in Fig. 4.4a for high coupling strength at L_{s_8}=4, $L_{s_{33}}$=21 are not present at L_{s_8}=21, $L_{s_{33}}$=4, which

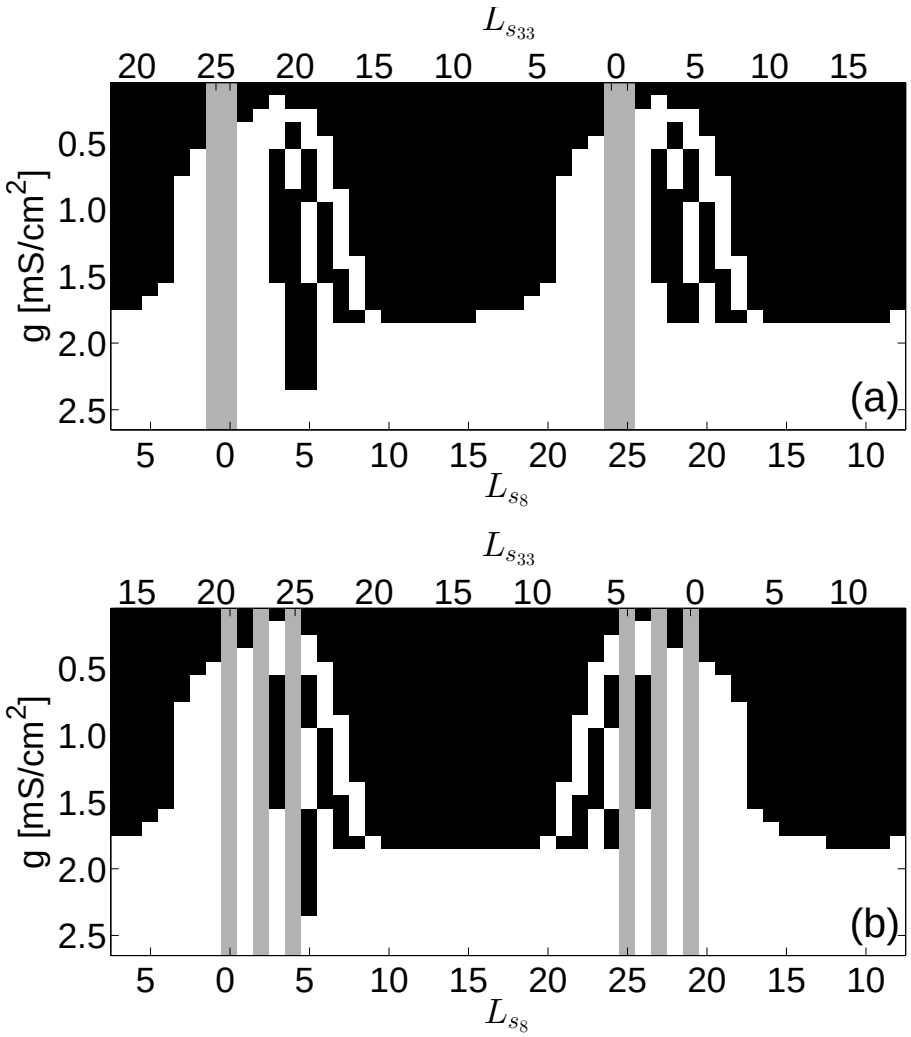

Figure 4.4. Binary map for two synapses, special case. Map of system states for varying coupling strength g and link length in the presence of two synaptic links, L_{s_8} and $L_{s_{33}}$, in an ML network of N=50 neurons. The two presynaptic neurons are held constant at j=8 and j=33 for all simulations. The two presynaptic neurons have a synapse in the direction of the traveling pulse for L_{s_8} and $L_{s_{33}}$ increases to the right (a). A synapse connecting the front to the back of the traveling pulse $L_{s_{33}}$ increases to the left (b). Initial condition, color coding, and other parameters are same as in Fig. 4.3a

is understandable. When the pulses first encounter is with a short synaptic link, the wide pulse will change to the narrow pulse and no chaos will be initiated, otherwise if the pulse travels to a long link chaos will initiate.

The bumps, where chaos initiated for small coupling strength, can interact with each other if the distance between the two postsynaptic neurons is changed. As before, the presynaptic neuron j=8 is connected to the postsynaptic neuron with a synapse of length L_{s_8}, and the presynaptic neuron j=33 is connected to a different postsynaptic neuron with

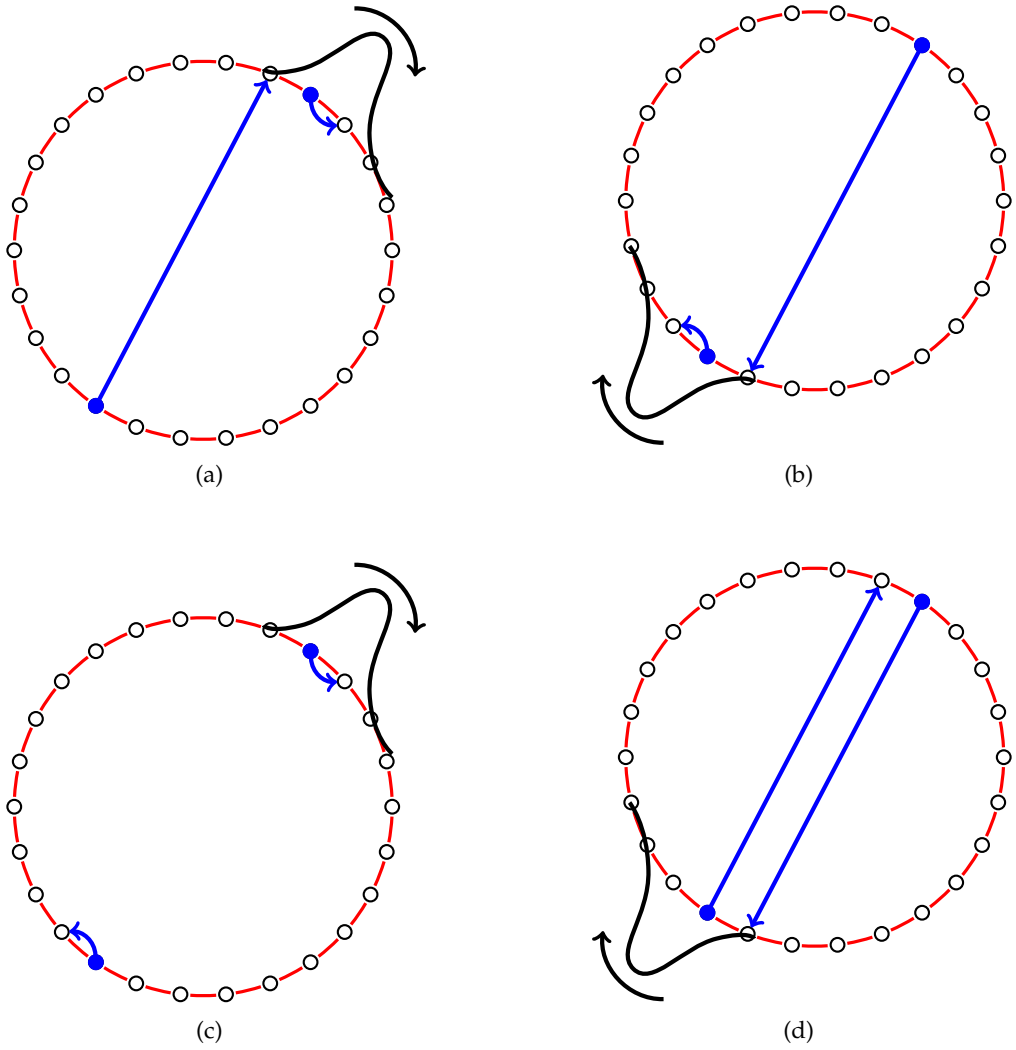

Figure 4.5. Traveling pulse schematic. Schematic of the network used in Fig. 4.6. Diffusively coupled network (red connections), in the presence of two synaptic links (blue arrows), having a traveling pulse solution as initial condition(black curve). (a, b) A network in the presence of a short link and a long link (ℓ is high). (c) A network in the presence of two short links (ℓ is low). (d) A network in the presence of two long links (ℓ is low).

a synapse of length $L_{s_{33}}$. The offset ℓ between L_{s_8} and $L_{s_{33}}$ was introduced to allow the network to have small and long links at the same time.

When the offset ℓ is high, one of the links is short and the other is long (Figs. 4.5a, b), the two bumps are the farthest possible (Fig. 4.4a), and the pulse affects each presynaptic neuron at different times. As the offset ℓ decreases, the difference in length between the two links decreases allowing the two bumps to move towards each other. When ℓ=1 the offset is low enough to have almost the same link length for both synapses (Figs. 4.5c, d).

The two bumps overlap, since the pulse reaches the presynaptic neuron at j=8 first, and is able to initiate chaos for short synapses, before it reaches the presynaptic neuron at j=33. This dependence on ℓ is the same for both, the wide pulse (Fig. 4.6a), as well as the narrow pulse (Fig. 4.6b).

This study shows that synaptic coupling can cause chaos initiation in the presence of a single pulse. Adding more synapses to the ring network influences chaos initiation insofar as the probability for a short synapse increases, and only such short synapses that cause coupling within a pulse allow chaos to start. This is expected to change, if a ring network is small, of the order of twice the width of a pulse, $N \leq 20$, such that all synapses transfer information continuously. Preliminary results for initially *two pulses in the presence of a single synapse* show that the onset of chaos is reached for a wider variety of coupling strength and link length than for the single pulse in Fig. 4.3a. The synapse influences the speed of propagation of one of the two pulses to eventually cause the moving of the pulse to a location were the onset of spatiotemporal chaos can happen. For a long link length, L_s, it can take a very long time for chaos to be initiated.

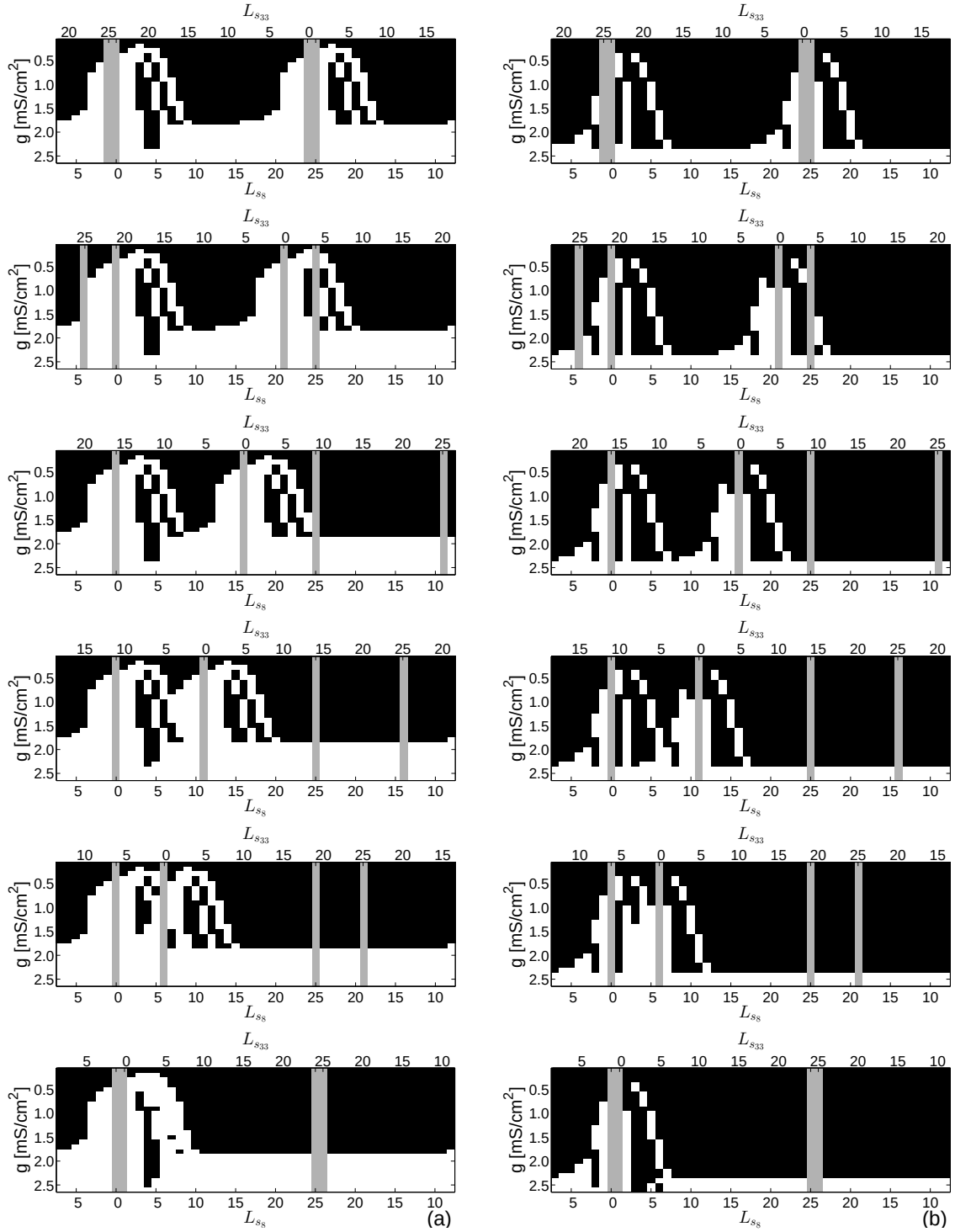

Figure 4.6. Binary map for chaos initiation in the presence of two synapses. Panel of system state maps for an initially (a) wide and (b) narrow pulse, in the presence of two synaptic links at varying synapse length, L_{s_8} and $L_{s_{33}}$, in an ML network of N=50 neurons. The offset ℓ between L_{s_8} and $L_{s_{33}}$, decreases from top to bottom (ℓ=24, ℓ=19, ℓ=14, ℓ=9, ℓ=4, ℓ=1). For other details see Fig. 4.3a.

Chapter 5
Conclusion

A diffusively coupled ring network of Morris-Lecar neurons presents transient spatiotemporal chaos before collapsing spontaneously and unpredictably to either a rest state or a pulse solution[10]. The lifetime of transient chaos was shown to increase exponentially with the network size[10]. After the collapse of chaos, the pulse solution exists in two configurations, a wide pulse or a narrow pulse. This study shows how transient chaos changes with the introduction of excitatory synaptic links that activate fast response AMPA receptors.

The majority of rapid excitatory synaptic transmission in the central nervous system is regulated by the AMPA receptor[13]. Epileptic synchronization was also attributed to this fast synaptic connection, making the AMPA receptor a target for epilepsy therapy[19].

When adding (unidirectional) excitatory synaptic links to a diffusively coupled network, the degree of coherence between neurons and the strength of chaos increases in comparison to the diffusive network. With the introduction of a single synaptic link, the network dynamics is rather similar to the diffusive case. When the number of synaptic links increases, the neuron dynamics has a larger Lyapunov exponent and a higher degree of phase coherence.

The lifetime of transient chaos is also affected by the presence of synaptic connections. For low to intermediate coupling strengths, the chaotic state will reach the collapse faster than for the diffusive case, while for high coupling strength the lifetime will increase exponentially with increasing link strength. A maximum lifetime for the transient was reached when the network was coupled with an intermediate number of synapses. The collapse state for high coupling strengths favors a global rest state over the pulse solution. In contrast to a purely diffusive network where each collapse state is asymptotic, the chaotic state can be initiated after the collapse to a pulse, if synaptic coupling is present. Previous studies show the weakening in neuron synchronization, and a taming of spatiotemporal chaos with increasing coupling strength in a network of only synaptically coupled neurons[20].

The onset of chaos can happen even with the addition of a single synapse at a low coupling strength and short link length. Above a critical coupling strength chaos is always initiated. Adding more synaptic links allows the parameters that initiate chaos to be distributed more complicated.

Studies of cognitive functions in the brain through fMRI and EEG[21] have shown that

the brain dynamics are transient and sequential. The brain transient dynamics consisting of the switching of metastable states has recently been hypothesized to be due to the presence of chains of saddle nodes, rather than due to a sequence of attractors[2].

Further study should focus on how the transient chaotic state changes when introducing a mixture of inhibitory and excitatory synapses, creating a more balanced network activity[22]. While the excitatory synapse can initiate chaos, an inhibitory synapse could perhaps facilitate the collapse. Inhibitory synapses through their negative feedback and slow synaptic current can control the neural firing rate, thus playing an important role for working memory function in the prefrontal cortex[23].

This study used a diffusively coupled ring network with unique synapses that could connect to each neuron only once. Further work should be concentrated on allowing more synapses per neuron, and on creating different network topologies[24], and by so doing mimicking a more realistic real-world neural network. Studies on rewiring of synaptic links between oscillatory neurons have shown that synchronization in neural activity can be promoted[25].

Bibliography

[1] Y. Lai and T. Tél, *Transient Chaos: complex dynamics on finite time scales*. Vol. 173. Springer, 2011.

[2] M. I. Rabinovich, R. Huerta, P. Varona, and V. S. Afraimovich. "Transient cognitive dynamics, metastability, and decision making." *PLoS Computational Biology* **4**, e1000072 (2008)

[3] K. McCann and P. Yodzis. "Nonlinear dynamics and population disappearances." *The American Naturalist* **144**, 873 (1994).

[4] L. Zhu, A. Raghu, and Y.-C. Lai. "Experimental observation of superpersistent chaotic transients." *Physical Review Letters* **86**, 4017 (2001).

[5] A. Wacker, S. Bose, and E. Schöll. "Transient spatio-temporal chaos in a reaction-diffusion model." *Europhysics Letters* **31**, 257 (1995).

[6] M. C. Strain and H. S. Greenside. "Size-dependent transition to high-dimensional chaotic dynamics in a two-dimensional excitable medium." *Physical Review Letters* **80**, 2306 (1998).

[7] R. Wackerbauer and K. Showalter. "Collapse of spatiotemporal chaos." *Physical Review Letters* **91**, 174103 (2003).

[8] B. Hof, J.Westerweel, T.M. Schneider, and B. Eckhardt. "Finite lifetime of turbulence in shear flows." *Nature* **443**, 7107 (2006).

[9] C. Morris and H. Lecar, "Voltage oscillations in the barnacle giant muscle fiber." *Biophysical Journal* **35**, 193 (1981).

[10] K. Keplinger and R. Wackerbauer. "Transient spatiotemporal chaos in the Morris-Lecar neuronal ring network." *Chaos* **24**, 013126 (2014).

[11] D. M. Durand, E.-H. Park, and A. L. Jensen. "Potassium diffusive coupling in neural networks." *Philosophical Transactions of the Royal Society B* **365**, 2347 (2010).

[12] P. Balenzuela and J. García-Ojalvo. "Role of chemical synapses in coupled neurons with noise." *Physical Review E* **72**, 021901 (2005).

[13] I. Song, and R. L. Huganir. "Regulation of AMPA receptors during synaptic plasticity." *Trends in Neurosciences* **25**, 578 (2002).

[14] K. Tsumoto, H. Kitajima, T. Yoshinaga, K. Aihara, and H. Kawakami. "Bifurcations in Morris-Lecar neuron model." *Neurocomputing* **69**, 293 (2006).

[15] G. B. Ermentrout and D. H. Terman. *Mathematical foundations of neuroscience*. Vol. 64. Springer, (2010).

[16] A. Destexhe, Z. F. Mainen, and T. J. Sejnowski. "Synthesis of models for excitable membranes, synaptic transmission and neuromodulation using a common kinetic formalism." *Journal of Computational Neuroscience* **1**, 195 (1994).

[17] Y. Kuramoto and I. Nishikawa. "Statistical macrodynamics of large dynamical systems. Case of a phase transition in oscillator communities." *Journal of Statistical Physics* **49**, 569 (1987).

[18] G. Benettin, L. Galgani, and J.-M. Strelcyn. "Kolmogorov entropy and numerical experiments." *Physical Review A* **14**, 2338 (1976).

[19] M. A. Rogawski. "AMPA receptors as a molecular target in epilepsy therapy." *Acta Neurologica Scandinavica* **127**, 9 (2013).

[20] Q. Y. Wang, Q. S. Lu, and G. R. Chen. "Ordered bursting synchronization and complex wave propagation in a ring neuronal network." *Physica A* **374**, 869 (2007).

[21] B. Horwitz, M. A. Tagamets, and A. R. McIntosh. "Neural modeling, functional brain imaging, and cognition." *Trends in Cognitive Sciences* **3**, 91 (1999).

[22] T. P. Vogels, H. Sprekeler, F. Zenke, C. Clopath, and W. Gerstner. "Inhibitory plasticity balances excitation and inhibition in sensory pathways and memory networks." *Science* **334**, 1569 (2011).

[23] X.-J. Wang. "Synaptic basis of cortical persistent activity: the importance of NMDA receptors to working memory." *The Journal of Neuroscience* **19**, 9587 (1999).

[24] D. S. Bassett and E. T. Bullmore, "Small-world brain networks." *The Neuroscientist* **12**, 512 (2006).

[25] H. T. Yu, J. Wang, Q. X. Liu, J. B. Sun, and H. F. Yu. "Delay-induced synchronization transitions in small-world neuronal networks with hybrid synapses." *Chaos, Solitons & Fractals* **48**, 68 (2013).